Chemical Science

ROYAL SOCIETY OF CHEMISTRY

EDGE ARTICLE

View Article Online
View Journal

Cite this: DOI: 10.1039/d6sc02183b

All publication charges for this article have been paid for by the Royal Society of Chemistry

Hacking a Brønsted photoacid to capture and directly release a Lewis acid: application to CO_2 photorelease

Berk Delibas,[a] Sumit Sahu,[a] Dani Cotton,[a] Hayden Harkins,[b] Andrew S. Petit,[b] Joaquín Rodríguez-López[cd] and Jahan M. Dawlaty*[a]

Received 16th March 2026
Accepted 21st May 2026

DOI: 10.1039/d6sc02183b

rsc.li/chemical-science

Controlling reactivity using light remains an important goal in chemistry. Since acid–base reactions are central to nearly all chemical phenomena, photoacids are important molecules for controlling reactivity. Conventional photoacids release protons upon excitation or generate a Lewis acid through light-induced structural changes. Here, we report a conceptually different mechanism of Lewis photoacidity that leverages the excited-state mechanisms of a Brønsted photoacid. It is well known that the Brønsted photoacid 2-naphthol releases a proton upon light absorption and converts to 2-naphtholate. We show that 2-naphtholate binds the Lewis-acidic CO_2 in the ground state and releases it upon photoexcitation. Through experimental and computational studies, we demonstrate that the spectroscopic characteristics and Förster cycle of this process are remarkably similar to those observed for proton release from 2-naphthol. This strategy provides a new approach for designing systems for reversible CO_2 capture and release and has potential for photochemistry of Lewis adducts beyond CO_2.

Introduction

Control over reactivity using external stimuli remains a central goal of modern chemistry. Among the available stimuli, light is uniquely powerful due to its versatility. Light can be used to trigger reactions with controlled timing,[1–4] is available as renewable energy in sunlight,[5–9] and enables a wide range of photochemical transformations.[10–12] Photoacids are particularly attractive in this context. Upon irradiation, this class of molecules undergoes an increase in acidity that can drive acid-dependent chemical reactions.[13] Several strategies have been developed to achieve photoacidity. First is the class of photoacids that undergo major structural changes that lead to more acidity,[14–19] for example merocyanines that undergo excited state photoisomerization.[20] Second is the class of excited state photoacids, such as naphthols and pyrenols,[21,22] where the molecule is more acidic in the excited state, without major structural changes.

While photoacids are most commonly discussed in terms of proton release, they can also be considered in the broader context of Lewis acidity. Such systems are known as photo-Lewis acid generators (PHLAGs).[19,23,24] Upon excitation, PHLAGs typically undergo irreversible structural changes that result in the release of a Lewis acid. The liberated Lewis acid can then increase the acidity of the solution through interactions with the solvent or directly participate in chemical transformations.[25–27]

In recent years, significant efforts have been devoted to overcome the high energy requirement for CO_2 release by using various stimuli including redox reactions triggered by electrodes,[28,29] humidity swings,[30] microwave irradiation,[31] pH swings,[32] and light.[33–37] Among these strategies, light-triggered CO_2 release is particularly appealing. Recently, merocyanine photoacids have been used by us and others[13,35,38,39] for the reversible capture and release of CO_2. Merocyanine releases a proton upon photoexcitation, which acidifies the solution, and shifts the CO_2 capture equilibrium towards release (Fig. 1, upper panel). Similarly, photobases have also been explored for light-controlled CO_2 capture and release.[13,34,40]

Here, we establish a general framework for reversible capture and release of Lewis acids using a canonical Brønsted photoacid. It is well-known that the Brønsted photoacid 2-naphthol can release a proton upon light absorption and convert to 2-naphtholate.[41–45] We show that the Lewis acidic CO_2 coordinates with 2-naphtholate and, analogous to a proton, can be directly ejected upon photoexcitation (Fig. 1). In this work CO_2 serves as a representative Lewis acidic molecule, but the conceptual framework is general and can in principle be extended to other Lewis acids. We provide experimental and computational

[a]Department of Chemistry, University of Southern California, Los Angeles, California 90089, USA
[b]Department of Chemistry and Biochemistry, California State University-Fullerton, Fullerton, California 92834, USA
[c]Department of Chemistry, University of Illinois Urbana–Champaign, Urbana, Illinois 61801, USA
[d]Beckman Institute for Advanced Science and Technology, University of Illinois Urbana–Champaign, Urbana, Illinois 61801, USA. E-mail: dawlaty@usc.edu

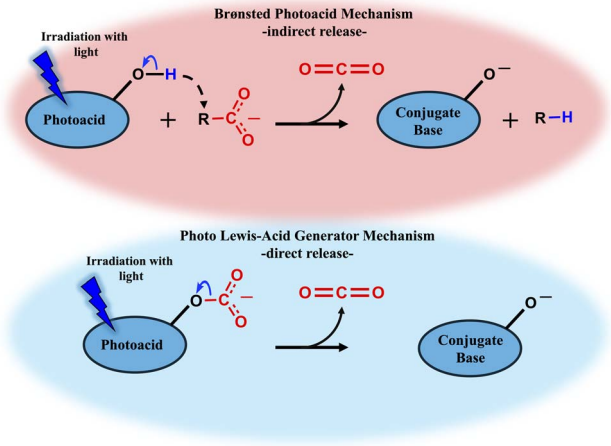

Fig. 1 Two approaches for using light to release CO_2. In the top panel, light releases a proton from a metastable Brønsted photoacid inducing a pH swing, which in turn affects the CO_2 equilibrium with the absorption agent. In the bottom panel we demonstrate our conceptually distinct approach, where CO_2 is adsorbed directly on the conjugate base of a Brønsted photoacid. We show that the photochemistry of proton ejection and CO_2 ejection are quite similar, thereby allowing direct photorelease of CO_2.

evidence for the thermodynamic feasibility of this process by constructing its Förster cycle and computationally demonstrating that excited state CO_2 release has a small energy barrier. Furthermore, both experiment and theory reveal surprising spectroscopic and thermodynamic similarities between 2-naphthol and the 2-naphtholate-CO_2 adduct.

The simplicity of this approach makes it a promising platform for exploring Brønsted photoacids as systems capable of direct Lewis acid release. Previous work by us had shown analogies between Brønsted and Lewis photobases.[46] The use of this approach may open new paths for interesting chemistries enabled by light-triggerable Lewis acid release beyond CO_2.[47]

Results and discussion

Characterization of the relevant species

We examined three substituted naphthols, 2-naphthol, 6-bromo-2-naphthol, and 6-methoxy-2-naphthol, for the reactivity of their conjugate bases towards CO_2 in tetrahydrofuran (THF). We have selected THF as our choice of solvent. THF was selected due to its ability to dissolve all the relevant chemical species (naphthols, naphtholates, and naphthylcarbonates) and its general unreactivity. Several other solvents such as DMSO, acetonitrile, triethylamine, and toluene were tried. However, THF proved to be the most suitable.

As shown in Fig. S14 in the SI, 6-methoxy-2-naphtholate is expected to have the highest affinity towards making an adduct with CO_2, which we attribute to the electron donating nature of the methoxy group. Further details on the ground state stability of these adducts can be found in Section S5 in the SI. Therefore, we will use 6-methoxy-2-naphthol as the molecule of choice for the experiments presented here. For ease of notation, 6-methoxy-2-naphthol, 6-methoxy-2-naphtholate, and 6-methoxy-2-naphthylcarbonate will be referred to as naphthol (NpOH), naphtholate (NpO^-), and naphthylcarbonate ($NpOCOO^-$) respectively for the rest of the paper.

Fig. 2 presents the reaction scheme and the FTIR, NMR, UV-vis, and fluorescence results for all relevant species. The FTIR spectrum (Fig. 2b) of NpOH (black dotted line) shows characteristic ring modes at ~1608 and ~1616 cm^{-1} for aromatic alcohols. Computational analysis, discussed in more detail below, suggests that the –OH bending mode is strongly coupled to these ring modes. The characteristic –OH stretch mode appears at ~3290 cm^{-1} (see inset, Fig. 2b). These features are in good agreement with assignments in the literature.[48] Upon deprotonation and formation of the NpO^- (blue dashed line), the –OH stretch mode is lost as expected. The ring modes of the NpO^- shift to lower frequencies relative to NpOH and overlap with other peaks as shown in Fig. S3 in the SI. Additionally a characteristic –CO stretch mode for NpO^- is observed at ~1591 cm^{-1}. After introducing CO_2 and forming $NpOCOO^-$, a large and distinctive peak at around ~1700 cm^{-1} is observed. This peak is well known[33,49] as the characteristic asymmetric stretch mode of the attached CO_2 fragment. In a previous study by our group we have established a correlation between the pK_a of alcohols and the frequencies of their carbonates.[33] Based on the pK_a of naphthol, our measured carbonate frequency matches the previously established trend (Fig. S5 in the SI). The spectrum of $NpOCOO^-$ shows that there is some leftover quantity of NpO^-, as evidenced by its characteristic peak at ~1591 cm^{-1}. Surprisingly, we observed that the features associated with the $NpOCOO^-$ ring mode (~1607 cm^{-1}) almost perfectly matched that of NpOH. This phenomenon, while unexpected, strongly suggests that the naphthalene ring is mostly agnostic to whether a Brønsted acidic proton or a Lewis acidic CO_2 is attached to the oxygen. It is important to note that ring mode at 1618 cm^{-1} is missing for $NpOCOO^-$. We attribute this fact to the lack of an –OH mode to couple with the ring modes in $NpOCOO^-$.

As described in more detail in Table S6 in the SI, our calculated harmonic vibrational frequencies provide additional support for the assignment of the FTIR spectra. Specifically, at the harmonic level, the highest-frequency bright ring modes of NpOH and $NpOCOO^-$ are very close to each other at 1680 cm^{-1} for NpOH and in a range of 1673–1679 cm^{-1} for $NpOCOO^-$. However, the corresponding mode of NpO^- is significantly red-shifted at 1653–1660 cm^{-1}. Note that the range of frequencies mentioned above for anionic species corresponds to the presence and absence of the Na^+ counter-ion coordination and their conformers. The Na^+ is present in the system because it is produced from the NaH reagent used to deprotonate NpOH. For this reason, in the simulation of all anions, we have considered both scenarios with and without explicit Na^+ ion pairing. Finally, we speculate that the experimental width of the carbonate stretch mode reflects, in part, variability in the solvent environment and position of the Na^+ counter ion. Therefore, in this work we will be reporting the values for the species with explicit contact pairing with Na^+.

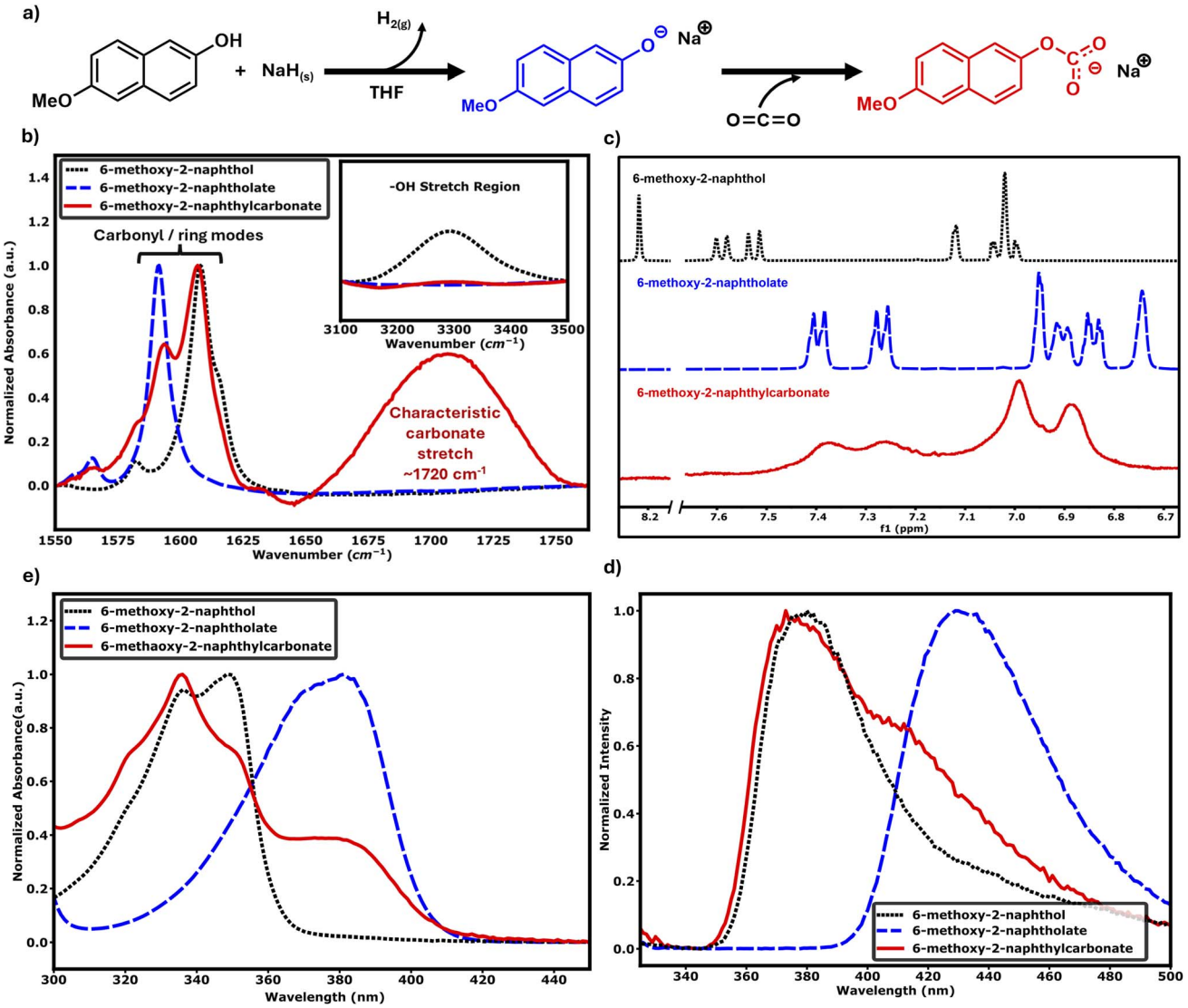

Fig. 2 Experimental reaction scheme (a) for 6-methoxy-2-naphthylcarbonate formation and FTIR (b), ^{1}H NMR (c), UV-vis (d), and fluorescence (e) spectra of each component of the reaction. 6-Methoxy-2-naphthol, 6-methoxy-2-naphtholate, and 6-methoxy-2-naphthylcarbonate in THF are depicted as black dotted lines, blue dashed lines, and red solid lines respectively.

To further establish the identity of the species, we present ^{1}H NMR (Fig. 2c) data. NpOH (black dotted line) yields a distinct –OH proton at 8.17 ppm and ring protons ranging from 7.54 to 6.89 ppm. As expected, upon formation of the NpO^{-} (blue dashed lines) the feature assigned to the –OH proton disappeared. Ring protons of NpO^{-} are up-shifted due to the more negative charge on the ring. Upon forming $NpOCOO^{-}$ (red solid line), the signal due to ring protons appears as broad peaks at a chemical shift that is in between that of NpOH and NpO^{-}. Importantly we do not see any signficant –OH proton feature upon formation of the $NpOCOO^{-}$ confirming that it is not significantly contaminated with NpOH. Even though two species ($NpOCOO^{-}$ and unreacted NpO^{-}) are present, as evidenced by the FTIR experiments, the ^{1}H NMR spectra show one set of peaks, which is likely due to the well-known fast exchange effect in NMR.[50,51] The large width of these peaks could be explained by the inhomogeneity of their highly ionic environments. The exact splittings on the NpO^{-} and especially $NpOCOO^{-}$ are not assignable due to significant broadening of the spectrum and overlap of signals.

Next, we show the UV-vis spectra of all three species (Fig. 2d). The NpOH spectrum (black dotted line) closely matches the photoacidic L_a band of various naphthols in the literature.[52] The NpO^{-} spectrum (blue dashed line) is red-shifted relative to NpOH which is consistent with the literature.[52] The $NpOCOO^{-}$ spectrum (red solid line) resembles that of NpOH, with features in the shorter wavelengths. As supported by the FTIR data shown above, the $NpOCOO^{-}$ solution also contains unreacted NpO^{-}. Correspondingly, the NpO^{-} peak is observed in the UV-vis spectrum. However, this peak is slightly shifted and broadened with respect to the pure NpO^{-} spectrum, which is likely due to the highly concentrated and ionic nature of the solution. We also observed a similar phenomenon when we intentionally mixed 2-naphthol and 2-naphtholate (SI Fig. S6).

We computationally explored the energetics and the electronic structure of the low lying electronic transitions for the relevant species in Fig. 2d. We note that different conformers of the species as well as the ion pairing with Na^+ in the solvent environment yielded different vertical excitation energies. These effects can be observed more clearly in the computational values reported in Tables S11 and S12 in the SI. We have calculated the $S_0 \rightarrow S_1$ vertical excitation energies of NpOH, NpO^- and $NpOCOO^-$ to be 3.81, 2.88–3.24, and 3.90–3.99 eV, respectively. As noted before, the range of energies corresponds to the presence and absence of Na^+ and its conformers. We note the similarity in vertical excitation energies between NpOH and $NpOCOO^-$. This similarity is consistent with the experimental results shown in Fig. 2d.

Finally, we present the emission spectra in Fig. 2e. Since the $NpOCOO^-$ sample has unreacted NpO^-, we chose 300 nm as our excitation wavelength since it has a small overlap with NpO^- absorption but significant overlap with $NpOCOO^-$. We used 300 nm excitation for all three species to keep the excitation energy constant between experiments. The NpOH (black dotted line) and NpO^- (blue dashed line) emissions have peaks at around 380 nm and 431 nm respectively and match well with values from the literature.[52] For $NpOCOO^-$ (red solid line) we observed two peaks in our emission data at 375 and 413 nm. These emissions are assigned to $NpOCOO^-$ and NpO^- respectively, consistent with other characterization studies discussed above. The channels for these emissions will be discussed later in the paper with additional computational evidence. As with the UV-vis spectra, the fluorescence assigned to $NpOCOO^-$ is remarkably similar to that of NpOH. Calculations reported in Table S11 in the SI support our assignments of the vertical $S_1 \rightarrow S_0$ transition energies for NpOH, NpO^-, and $NpOCOO^-$ as 3.38, 2.50–2.83, and 3.17–3.53 eV, respectively, with the range of energies corresponding to the presence and absence of Na^+ and its conformers. We again note that vertical transition energies for emission between NpOH and $NpOCOO^-$ are very similar compared to that of NpO^-.

In analyzing the emission spectrum of $NpOCOO^-$, we note that the NpO^- emission in this sample appears as a shoulder and is significantly blue-shifted compared to pure NpO^-. Since only the emission of $NpOCOO^-$ is required to construct the Förster cycle, further explanation of this effect is not needed. Possible reasons for the blue shifted NpO^- peak are discussed in Section S2.3 in the SI.

The other molecules, 2-naphthol and 6-bromo-2-naphthol, also exhibited similar trends in their spectra which is supported by computational results that reveal similar patterns in the harmonic vibrational frequencies, vertical and adiabatic energy gaps, and natural transition orbitals between all of the systems. Further information on their spectra can be found in Section S5 in the SI.

Construction of the Förster cycle for napthylcarbonate

Fig. 3a presents the natural transition orbitals (NTOs) associated with the $S_0 \rightarrow S_1$ transition for all 3 species at the ground state optimized geometry. For all three molecules, the electronic transitions show a clear $\pi \rightarrow \pi^*$ character. Analysis shown in Fig. S22 and S25 in the SI reveals that the electronic character of the S_1 state is largely unaffected by the presence or absence of a Na^+ ion. Importantly, we note that the NTOs of NpOH and $NpOCOO^-$ are remarkably similar. This is consistent with our previous analysis where we showed that $NpOCOO^-$ and NpOH have very similar spectroscopic signatures. Collectively, our analysis shows that the influence of the Lewis acidic CO_2 on the electronic structure of the rings is similar to the influence of the Brønsted acidic proton. Therefore, we postulate that the mechanisms which govern the naphthol Brønsted photoacidity will be similar to those of Lewis photoacidity.

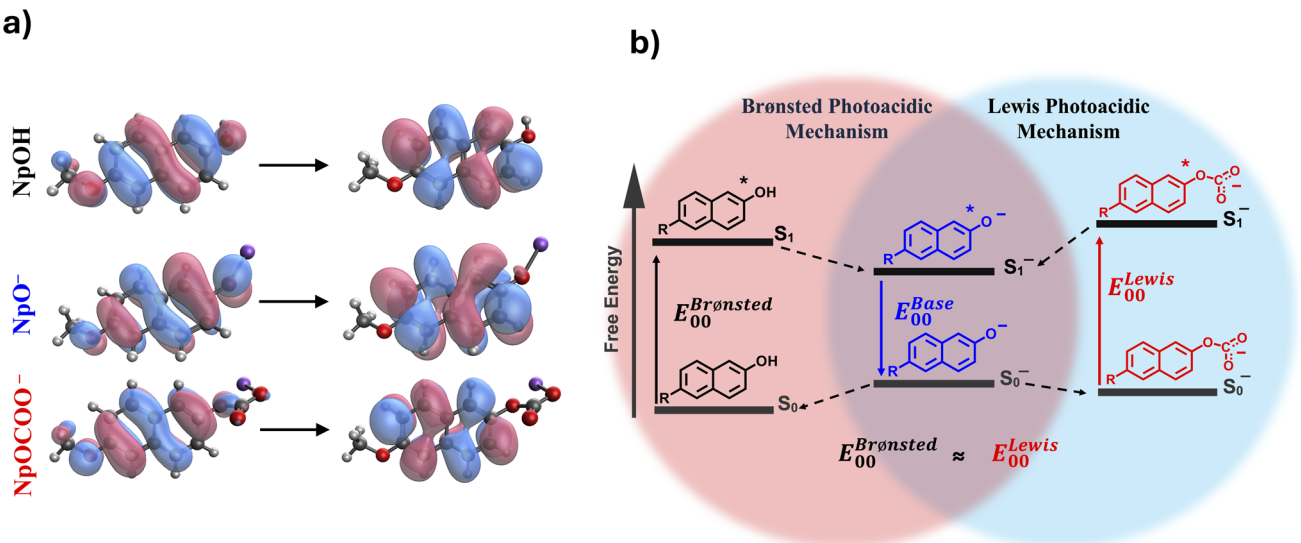

Fig. 3 The natural transition orbitals (NTOs) (a) for the $S_0 \rightarrow S_1$ transition of NpOH, NpO^- Na^+, and $NpOCOO^-$ Na^+ at the ground state optimized geometry and plotted with an isovalue of 0.06. Scheme (b) shows the Förster cycles for Brønsted and Lewis photo-acidic naphthols. Both Brønsted and Lewis photoacid mechanisms show nearly identical behaviour as proved experimentally and computationally in this work.

To demonstrate the photoacidity of the Lewis adduct, we use the above experimental and computational results to construct the Lewis Förster cycle for the $NpOCOO^-$ and NpO^- pair. We show that similar to the thermodynamic drive for NpOH to release its proton in the excited state, $NpOCOO^-$ also has the drive to release its CO_2 in its excited state. For constructing the Lewis Förster cycle for the $NpOCOO^-$ and NpO^- pair, we make assumptions similar to those made for the canonical Brønsted Förster cycles.[41,53]

Fig. 3b shows the Lewis Förster cycle along with the Brønsted Förster cycle for comparison. The adiabatic energies have been experimentally estimated by finding the intersection points between the absorption and emission spectra, which is a standard method in the field of excited state proton transfer.[53] The details are reported in Section S3 in the SI. Computational adiabatic energies are found by evaluating $E_{00} = E_{00}^{(S_1)} - E_{00}^{(S_0)}$, where $E_{00}^{(S_0)}$ is the ground state energy calculated at the S_0-optimized geometry while $E_{00}^{(S_1)}$ is the energy of the S_1 state calculated at the excited state optimized geometry. Using both the adiabatic energies for $NpOCOO^-$ and NpO^-, the difference in pK_{CO_2} between the ground and excited states can be calculated using the following equation:

$$\Delta pK_{CO_2} = pK^*_{CO_2} - pK_{CO_2} = \frac{E_{00}^{NpO^-} - E_{00}^{NpOCOO^-}}{2.303RT} \quad (1)$$

Note that a negative sign of ΔpK_{CO_2} corresponds to an increased drive for CO_2 release in the excited state.

Because the adiabatic energy gaps for NpOH and $NpOCOO^-$ are similar in THF at room temperature, the experimental $\Delta pK_a \approx -6.3$ and $\Delta pK_{CO_2} \approx -6.7$ are similar. Importantly, ΔpK_{CO_2} is significantly less than 0, demonstrating that this molecule is a Lewis photoacid with a thermodynamic driving force to release CO_2 upon photoexcitation. As shown in Table S17 in the SI, our computational analysis also demonstrates Lewis photoacidity, although we overestimate the magnitude of the thermodynamic driving force with calculated $\Delta pK_a = -9.33$ and $\Delta pK_{CO_2} = -11.93$. The computational overestimate is likely due to lack of explicit solvation and an ionic environment. For example, if we neglect the presence of a contact ion pair with Na^+, the deviation from the experiment becomes even larger.

We now consider the physical insight into the origin of the photorelease of CO_2 from $NpOCOO^-$. The NTOs shown in Fig. 3a indicate that the $S_0 \rightarrow S_1$ electronic excitation shifts electron density away from the oxygen atom that binds the CO_2, weakening the dative bond that holds the Lewis adduct together. Löwdin population analysis using the transition density matrix reported in Tables S20 and S21 in the SI confirms loss of electron density at this oxygen atom for both NpOH and $NpOCOO^-$ after the electronic excitation. Additional insights into the photoacidity of $NpOCOO^-$ are achieved using energy decomposition analysis (EDA) summarized in Fig. S32 and Table S22 in the SI. Photoexcitation reduces Pauli repulsion, stabilizing the Lewis adduct. However, all attractive intermolecular interactions decrease in magnitude with electronic excitation. This is especially true for the polarization and classical electrostatics components of the interaction energy. Overall, the stabilization caused by reduced Pauli repulsion is overwhelmed by the collective weakening of all attractive components of the interaction energy, resulting in weaker dative bonding in the S_1 state than in S_0.

Direct photorelease of CO_2 from naphthylcarbonate

The Förster cycle presented in the previous section proves a favorable thermodynamic driving force for CO_2 release in the excited state. However, the existence of a thermodynamic driving force does not prove that the process is kinetically feasible. For example, if excited state CO_2 release involves a substantial energy barrier, Lewis photoacidity may not kinetically compete with other decay channels. In this section, we present evidence that the barrier for CO_2 release in the excited state is small and that photorelease of CO_2 can be achieved experimentally.

Fig. 4a compares reaction coordinate diagrams for CO_2 release from $NpOCOO^-$ on S_0 (gray) and S_1 (red) potential energy surfaces. Excitation to S_1 significantly increases the thermodynamic driving force for CO_2 release while also reducing the transition state barrier. The presence of an approximately 3 kcal mol^{-1} barrier for the excited state allows CO_2 release but also ensures fluorescence from $NpOCOO^-$. Importantly, this is consistent with the experimental observation of emission from $NpOCOO^-$. It is worth noting that in the absence of a contact ion pair, no barrier for CO_2 release is observed in the calculations (SI Fig. S36). Fig. 4b shows potential energy curves for the S_0, S_1, and T_1 states along the pathway for light-driven release of CO_2 from $NpOCOO^-$. These geometries were obtained from a relaxed scan stretching the C–O dative bond on S_1. This analysis demonstrates that CO_2 release is adiabatic, with the S_0 and T_1 states remaining well-separated from S_1 throughout. Additional analysis shown in Section S5 in the SI indicates that no higher-lying singlet or triplet states become close in energy to S_1 as the dative bond is stretched. Importantly, the adiabaticity of the excited-state CO_2 release is consistent with the experimental observation that excitation of $NpOCOO^-$ results in emission from NpO^- once CO_2 is released in the excited state. Even though we do not have absolute experimental evidence that the NpO^- emission arises from $NpOCOO^-$ that has lost its CO_2 in the excited state, the fact that we have significant NpO^- emission along with $NpOCOO^-$ hints that such an emission channel is possible.

Next, to prove photorelease of CO_2, we used a sealed FTIR cell containing either the 6-methoxy or the unsubstituted 2-naphthylcarbonate solution in THF and 10% (v/v) triethylamine (TEA) solution. TEA was used to stabilize the carbonate and limit the effects of water contamination. The cell was illuminated with 340 nm LED light while the FTIR spectra were being continuously measured. We tracked the carbonate peak of the $NpOCOO^-$ to measure its concentration in cycles of light on and off (Fig. 5). For both samples we observe sharp decreases in carbonate peak intensity upon irradiation, which shows that the $NpOCOO^-$ adduct breaks with light. Importantly, we also observed the regeneration of the $NpOCOO^-$ peak during the dark parts of the cycles. In the experiments shown there is an

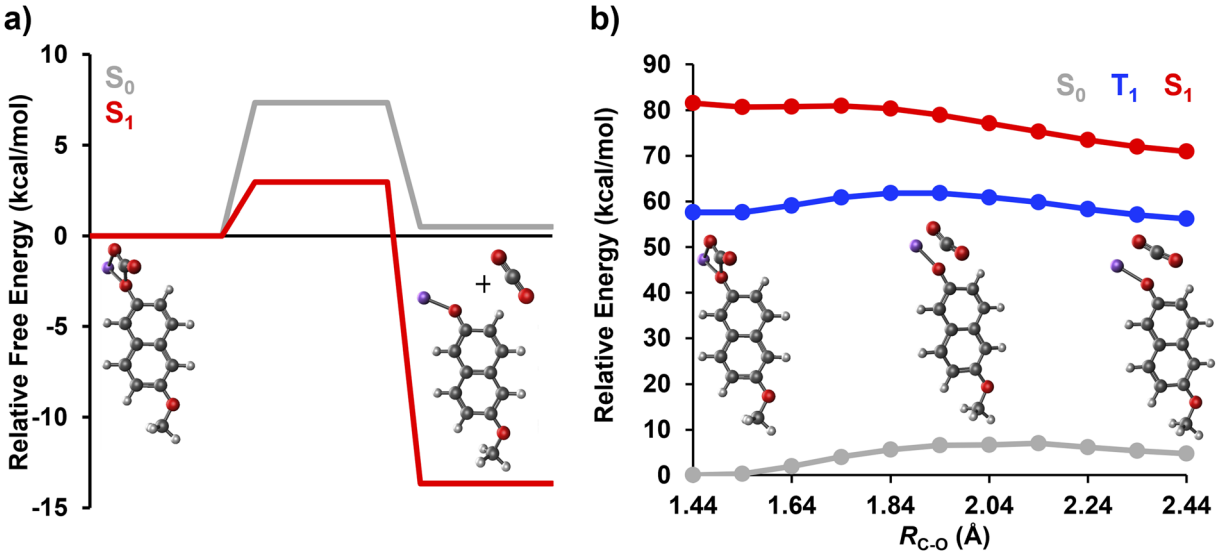

Fig. 4 Panel (a) compares the reaction coordinate diagrams for CO_2 release from $NpOCOO^-$ + Na^+ on S_0 (gray line) and S_1 (red line) as calculated at the ωB97M-V/def2-QZVPD//ωB97X-D/def2-SVPD level of theory with a ROKS treatment of the excited state. Panel (b) shows potential energy curves associated with stretching the dative bond in $NpOCOO^-$ + Na^+, R_{C-O}, for the S_0, S_1, and T_1 states. The geometries were obtained from a relaxed scan performed on S_1 using the ROKS-ωB97X-D/def2-SVPD level of theory while the energies were evaluated using ADC(2)/def2-TZVPD. Insets show representative geometries along the scan.

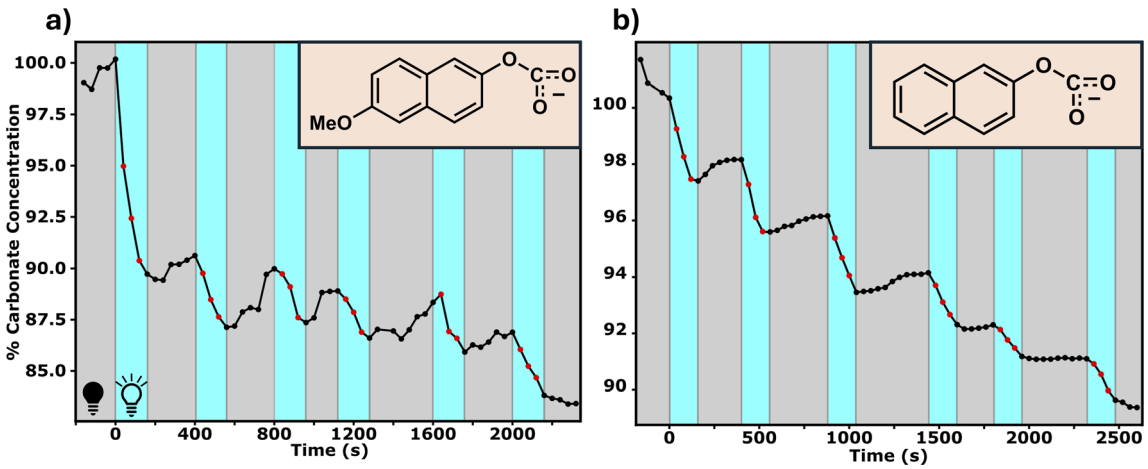

Fig. 5 Relative change in naphthylcarbonate concentration with respect to time for 6-methoxy-2-naphthylcarbonate (a) and 2-naphthylcarbonate (b) in THF. The cyan shade corresponds to irradiation with 340 nm light and dark shade corresponds to no illumination. A clear decrease in carbonate concentration upon irradiation with light and recovery of carbonate concentration in the dark is observed.

overall decrease in carbonate concentrations as not all the carbonate is regenerated once the light is turned off. We attribute this to the following. The FTIR cells used in the experiments are not completely airtight. Therefore, some of the released CO_2 is able to escape the solution and is unable to be recaptured. Additionally, water contaminates the system over time, reducing the available naphtholates to recapture the CO_2 in the absence of a strong enough base. However, we propose that it may be possible to use this approach even in aqueous media. Further discussion about this topic can be found in Section S2.4 in the SI. Photobleaching under irradiation is also possible. However, we do not believe that this is the driving factor for the irreversibility in our system.

The above results both point to not only the existence of a thermodynamic driving force for the photorelease of CO_2 but also show that it can be achieved experimentally. Therefore, we show that release of the Lewis acidic CO_2 in the excited state is analogous to that of a Brønsted photoacid. While photorelease of Lewis acids has been demonstrated before,[47] in this work we show that conjugate base of a Brønsted photoacid can coordinate with a Lewis acid and release it upon photoexcitation.

As mentioned above we have also studied unsubstituted and bromo-substituted naphthols. Their spectra and comparative analysis can be found in SI Section S2. Although, bromo-substituted naphthol did not have favorable conditions for experimental Förster cycle analysis it is important to note that

methoxy-substituted naphthol showed smaller drive for CO_2 release in its excited state compared to the unsubstituted naphthol (ΔpK_{CO_2} −6.7 and −8.2 respectively). This trend was also observed computationally across a larger variety of substituents (SI Section S5). Such behavior in photoacidity with electron-donating/withdrawing substitutions was studied by us and others in different systems.[46,54–56] It is interesting to note that our system follows a similar trend to canonical photoacids.

Conclusion

In this study, we demonstrate a new approach to light-triggered Lewis acid release. We have shown, both experimentally and computationally, the analogies between Brønsted and Lewis photoacidic pathways. This work lays the foundation for using Brønsted photoacids as platforms for releasing Lewis acids without requiring the often irreversible structural changes associated with conventional photoacids. Our approach offers some advantages over the conventional photo-Lewis acid generators by reversibly releasing the Lewis acid in the excited state.

Additionally, the Lewis Förster cycle constructed in this work has a lot of similarities to its Brønsted counterpart. We anticipate that the Lewis Förster cycle may be tunable in analogy to the Brønsted photocycles that have been reported before.[57–59] Our work may be extendable to photorelease of other Lewis acids, especially those that are relevant for catalyzing reactions, such as BF_3.[60] However, interaction of the stronger Lewis acids, such as BF_3, may prevent easy photorelease, and further work may be necessary for finding suitable systems.

While this study focuses on a new conceptual approach for releasing CO_2 we believe that it can be built upon and be integrated in large scale CO_2 capture and release systems. Furthermore, our approach differs from previously reported light-driven CO_2 release strategies that rely on metastable photoacids, such as merocyanines, which operate through structural changes that induce a pH shift and indirectly alter the CO_2 equilibrium. In contrast, the system presented here is based on a classical photoacid scaffold, where light directly weakens the interaction between the conjugate base and CO_2, enabling stoichiometric photorelease without relying on bulk pH changes. Given the electronic structure similarity between the excited states of $NpOCOO^-$ and NpOH, it would be interesting to compare the ultrafast kinetics of their respective dissociations in future studies.

Finally, in our computations we have observed that the barrier for CO_2 release in the excited state is dependent on the contact pairing and the solvent environment. We believe that by changing the counter ion used in this experiment it may be possible to tune the release rate of CO_2 with light.

Author contributions

JMD conceptualized and supervised the study and analysed the data. BD conceptualized the study, performed spectroscopy experiments, and analysed the data. SS conducted spectroscopic experiments and analysed the data. BD and SS wrote the original draft of the manuscript. DC conceptualized the study and conducted initial experiments. HH and ASP performed the theoretical calculations, analysed the results, and contributed to manuscript writing. JRL analysed the data. All authors discussed the results, contributed to the writing of the manuscript, and approved the final version.

Conflicts of interest

There are no conflicts to declare.

Data availability

Data used in this work are available upon request.

Supplementary information (SI): additional figures and discussions referenced. See DOI: https://doi.org/10.1039/d6sc02183b.

Acknowledgements

JMD and BD were supported under grant DE-SC0022173 from the Department of Energy (DOE) and grant CHE 2154493 from the National Science Foundation (NSF). ASP and HH acknowledge the donors of the Petroleum Research Fund, administered by the American Chemical Society (66491-UR4). Computational resources were provided through the Titan Supercomputing Center at California State University, Fullerton. We have benefited greatly from discussions with Prof. Veronica Augustyn at North Carolina State University.

References

1 S. Aubert, M. Bezagu, A. C. Spivey and S. Arseniyadis, *Nat. Rev. Chem.*, 2019, **3**, 706–722.
2 S. Jia and E. Sketten, *ACS Chem. Biol.*, 2022, **17**, 3255–3269.
3 T. Hwang and K. Hsiao, *Addit. Manuf.*, 2025, **114**, 105021.
4 R. Göstl, A. Senf and S. Hecht, *Chem. Soc. Rev.*, 2014, **43**, 1982–1996.
5 S. Luo, X. Ren, H. Lin, H. Song and J. Ye, *Chem. Sci.*, 2021, **12**, 5701–5719.
6 N. S. Lewis and D. G. Nocera, *Proc. Natl. Acad. Sci. U. S. A.*, 2006, **103**, 15729–15735.
7 D. Gust, T. A. Moore and A. L. Moore, *Acc. Chem. Res.*, 2009, **42**, 1890–1898.
8 D. G. Nocera, *Acc. Chem. Res.*, 2012, **45**, 767–776.
9 D. M. Schultz and T. P. Yoon, *Science*, 2014, **343**, 1239176.
10 C. K. Prier, D. A. Rankic and D. W. C. MacMillan, *Chem. Rev.*, 2013, **113**, 5322–5363.
11 D. A. Nicewicz and D. W. C. MacMillan, *Science*, 2008, **322**, 77–80.
12 T. P. Yoon, M. A. Ischay and J. Du, *Nat. Chem.*, 2010, **2**, 527–532.
13 A. Yucknovsky and N. Amdursky, *Angew. Chem., Int. Ed.*, 2025, **64**, e202422963.
14 C. J. Martin, G. Rapenne, T. Nakashima and T. Kawai, *J. Photochem. Photobiol., C*, 2018, **34**, 41–51.

15 A. Y. Khalimon, W. E. Piers, J. M. Blackwell, D. J. Michalak and M. Parvez, *J. Am. Chem. Soc.*, 2012, **134**, 9601–9604.
16 R. Klajn, *Chem. Soc. Rev.*, 2013, **43**, 148–184.
17 Z. Shi, P. Peng, D. Strohecker and Y. Liao, *J. Am. Chem. Soc.*, 2011, **133**, 14699–14703.
18 Y. Liao, *Acc. Chem. Res.*, 2017, **50**, 1956–1964.
19 A. Y. Khalimon, B. K. Shaw, A. J. V. Marwitz, W. E. Piers, J. M. Blackwell and M. Parvez, *Dalton Trans.*, 2015, **44**, 18196–18206.
20 L. Wimberger, S. K. K. Prasad, M. D. Peeks, J. Andréasson, T. W. Schmidt and J. E. Beves, *J. Am. Chem. Soc.*, 2021, **143**, 20758–20768.
21 J. Saway, Z. M. Salem and J. J. Badillo, *Synthesis*, 2021, **53**, 489–497.
22 E. Pines, in *The Chemistry of Phenols*, John Wiley & Sons, Ltd, 2003, pp. 491–527.
23 C. J. Martin, G. Rapenne, T. Nakashima and T. Kawai, *J. Photochem. Photobiol., C*, 2018, **34**, 41–51.
24 R. Mizutsu, R. Asato, C. J. Martin, M. Yamada, Y. Nishikawa, S. Katao, M. Yamada, T. Nakashima and T. Kawai, *J. Am. Chem. Soc.*, 2019, **141**, 20043–20047.
25 *Lewis Acids in Organic Synthesis*, Wiley, https://www.wiley.com/en-us/Lewis+Acids+in+Organic+Synthesis-p-9783527618309, accessed 13 March 2026.
26 J. Becica and G. E. Dobereiner, *Org. Biomol. Chem.*, 2019, **17**, 2055–2069.
27 H. Yamamoto and K. Futatsugi, *Angew. Chem., Int. Ed.*, 2005, **44**, 1924–1942.
28 A. M. Zito, L. E. Clarke, J. M. Barlow, D. Bím, Z. Zhang, K. M. Ripley, C. J. Li, A. Kummeth, M. E. Leonard, A. N. Alexandrova, F. R. Brushett and J. Y. Yang, *Chem. Rev.*, 2023, **123**, 8069–8098.
29 J. H. Rheinhardt, P. Singh, P. Tarakeshwar and D. A. Buttry, *ACS Energy Lett.*, 2017, **2**, 454–461.
30 T. Wang, K. S. Lackner and A. Wright, *Environ. Sci. Technol.*, 2011, **45**, 6670–6675.
31 T. H. Lim, J. E. Foster, B. R. Ellis and S. J. Skerlos, *Environ. Res. Lett.*, 2024, **19**, 034002.
32 H. Seo, M. P. Nitzsche and T. A. Hatton, *Acc. Chem. Res.*, 2023, **56**, 3153–3164.
33 B. Delibas, D. Cotton, K. P. Sudhakaran and J. M. Dawlaty, *ChemSusChem*, 2024, e202402288.
34 M. Purdy, A. Y. Wang, M. C. Drummer, D. G. Nocera and R. Y. Liu, *ChemRxiv*, 2025, preprint, DOI: 10.26434/chemrxiv-2025-gpsx8.
35 A. M. Alfaraidi, B. Kudisch, N. Ni, J. Thomas, T. Y. George, K. Rajabimoghadam, H. J. Jiang, D. G. Nocera, M. J. Aziz and R. Y. Liu, *J. Am. Chem. Soc.*, 2023, **145**, 26720–26727.
36 H. Seo, J. Schretter, M. Massen-Hane and T. A. Hatton, *J. Am. Chem. Soc.*, 2024, **146**, 26777–26785.
37 B. I. Z. Ahmad, K. Z. Colley, A. J. Musser and P. J. Milner, *Chem*, 2025, **11**(9), 102583.
38 A. De Vries, K. Goloviznina, M. Reiter, M. Salanne and M. R. Lukatskaya, *Chem. Mater.*, 2024, **36**, 1308–1317.
39 D. Cotton, T. Khuu, K. Takematsu, B. Delibas and J. M. Dawlaty, *J. Phys. Chem. Lett.*, 2024, **15**, 7782–7787.
40 J. Einkauf, D. Stamberga, N. Bhattacharjee, Y.-Z. Ma, B. Vyacheslav and R. Custelcean, *ChemRxiv*, 2025, preprint, DOI: 10.26434/chemrxiv-2025-w461z.
41 Th. Förster and Z. Für Elektrochem, *Angew. Phys. Chem.*, 1950, **54**, 531–535.
42 L. Genosar, P. Leiderman, N. Koifman and D. Huppert, *J. Phys. Chem. A*, 2004, **108**, 1779–1789.
43 N. Agmon, *J. Phys. Chem. A*, 2005, **109**, 13–35.
44 L. M. Tolbert and K. M. Solntsev, *Acc. Chem. Res.*, 2002, **35**, 19–27.
45 W. R. Laws and L. Brand, *J. Phys. Chem.*, 1979, **83**, 795–802.
46 M. J. Voegtle and J. M. Dawlaty, *J. Am. Chem. Soc.*, 2022, **144**, 8178–8184.
47 A. Y. Khalimon, W. E. Piers, J. M. Blackwell, D. J. Michalak and M. Parvez, *J. Am. Chem. Soc.*, 2012, **134**, 9601–9604.
48 R. S. Premachandran, S. Banerjee, X.-K. Wu, V. T. John, G. L. McPherson, J. Akkara, M. Ayyagari and D. Kaplan, *Macromolecules*, 1996, **29**, 6452–6460.
49 B. Delibas, K. J. Kron, D. E. Cotton, N. Salazar, S. M. Sharada and J. M. Dawlaty, *J. Phys. Chem. A*, 2023, **127**, 5162–5170.
50 J. Frahm, *Ber. Bunsenges. Phys. Chem.*, 1982, **86**, 873.
51 H. M. McConnell, *J. Chem. Phys.*, 1958, **28**, 430–431.
52 L. F. Cotter, P. J. Brown, R. C. Nelson and K. Takematsu, *J. Phys. Chem. B*, 2019, **123**, 4301–4310.
53 Z. R. Grabowski and A. Grabowska, *Z. Phys. Chem.*, 1976, **101**, 197–208.
54 K. U. Jagushte, N. Sadhukhan, H. P. Upadhyaya and S. Dutta Choudhury, *J. Phys. Chem. B*, 2023, **127**, 9788–9801.
55 J. Liu, W. Tang, L. Sheng, Z. Du, T. Zhang, X. Su and S. X.-A. Zhang, *Chem.–Asian J.*, 2019, **14**, 438–445.
56 E. W. Driscoll, J. R. Hunt and J. M. Dawlaty, *J. Phys. Chem. Lett.*, 2016, **7**, 2093–2099.
57 E. W. Driscoll, J. R. Hunt and J. M. Dawlaty, *J. Phys. Chem. Lett.*, 2016, **7**, 2093–2099.
58 J. R. Hunt and J. M. Dawlaty, *J. Phys. Chem. A*, 2018, **122**, 7931–7940.
59 B. T. Psciuk, M. Prémont-Schwarz, B. Koeppe, S. Keinan, D. Xiao, E. T. J. Nibbering and V. S. Batista, *J. Phys. Chem. A*, 2015, **119**, 4800–4812.
60 G. K. S. Prakash, T. Mathew, E. R. Marinez, P. M. Esteves, G. Rasul and G. A. Olah, *J. Org. Chem.*, 2006, **71**, 3952–3958.